SCIENCE CHINA
Life Sciences

•RESEARCH PAPER•

December 2019 Vol.62 No.12: 1670–1682
https://doi.org/10.1007/s11427-018-9393-8

Supercritical fluid-assisted controllable fabrication of open and highly interconnected porous scaffolds for bone tissue engineering

Hanxiao Tang[1], Ranjith Kumar Kankala[1,2,3], Shibin Wang[1,2,3] & Aizheng Chen[1,2,3*]

[1]*College of Chemical Engineering, Huaqiao University, Xiamen 361021, China;*
[2]*Institute of Biomaterials and Tissue Engineering, Huaqiao University, Xiamen 361021, China;*
[3]*Fujian Provincial Key Laboratory of Biochemical Technology (Huaqiao University), Xiamen 361021, China*

Received October 20, 2018; accepted December 10, 2018; published online Apirl 16, 2019

Recently tremendous progress has been evidenced by the advancements in developing innovative three-dimensional (3D) scaffolds using various techniques for addressing the autogenous grafting of bone. In this work, we demonstrated the fabrication of porous polycaprolactone (PCL) scaffolds for osteogenic differentiation based on supercritical fluid-assisted hybrid processes of phase inversion and foaming. This eco-friendly process resulted in the highly porous biomimetic scaffolds with open and interconnected architectures. Initially, a 2^3 factorial experiment was designed for investigating the relative significance of various processing parameters and achieving better control over the porosity as well as the compressive mechanical properties of the scaffold. Then, single factor experiment was carried out to understand the effects of various processing parameters on the morphology of scaffolds. On the other hand, we encapsulated a growth factor, i.e., bone morphogenic protein-2 (BMP-2), as a model protein in these porous scaffolds for evaluating their osteogenic differentiation. *In vitro* investigations of growth factor loaded PCL scaffolds using bone marrow stromal cells (BMSCs) have shown that these growth factor-encumbered scaffolds were capable of differentiating the cells over the control experiments. Furthermore, the osteogenic differentiation was confirmed by measuring the cell proliferation, and alkaline phosphatase (ALP) activity, which were significantly higher demonstrating the active bone growth. Together, these results have suggested that the fabrication of growth factor-loaded porous scaffolds prepared by the eco-friendly hybrid processing efficiently promoted the osteogenic differentiation and may have a significant potential in bone tissue engineering.

supercritical foaming, polycaprolactone, bone tissue engineering, osteogenic differentiation, bone morphogenic protein-2

Citation: Tang, H., Kankala, R.K., Wang, S., and Chen, A. (2019). Supercritical fluid-assisted controllable fabrication of open and highly interconnected porous scaffolds for bone tissue engineering. Sci China Life Sci 62, 1670–1682. https://doi.org/10.1007/s11427-018-9393-8

INTRODUCTION

Currently, the clinically-accepted treatment strategies such as mounting of autologous, and allogenous xenografts have become potential therapeutic approaches for treating bone defects (Brydone et al., 2010). However, the application of these approaches is limited due to several concerns such as the risk of acute immune rejection, prone to infection, antigenicity, and severe pain and donor site morbidity, among others, which remained as highly challenging for surgeons (Cabraja and Kroppenstedt, 2012; Oryan et al., 2014). Recently, tissue engineering (TE) has garnered enormous interest from researchers as a promising alternative due to the upsurge in demand for organ replacement therapies and a shortage of donors (Kankala et al., 2018a; Moshiri and Oryan, 2012). Conceptually, this field predominantly involves the generation of well-designed biomimetic tissue substitutes in three dimensional (3D) orientation and achieve a better control over the scaffold's architecture for replacing the malfunctioned organs or tissue constructs to recreate or re-

*Corresponding author (email: azchen@hqu.edu.cn)

store their function, since the native tissues are quite intricate as they are composed of complex extracellular matrix (ECM) with different cell types and various signaling cues In this framework, these 3D architectures are often used to cultivate various cells types, including stem cells for engineering the functional tissue substitutes (Lenas and Ikonomou, 2018; Cao et al., 2018; Zhao et al., 2017; Hegde et al., 2013). Nonetheless, a few of the characteristic features are highly required in the 3D matrices of the scaffold for efficient growth and differentiation of cells. More often, the critical requirements for TE scaffolds include high porosity, with open and interconnected pores, and sufficient mechanical strength that facilitate sufficient space for cell infiltration, growth, and differentiation, along with the nutrient diffusion and removal of metabolic waste during tissue maturation (Chen et al., 2017; Custódio et al., 2014; Kim et al., 2017; Zeltinger et al., 2001). Recently, tremendous progress has evidenced the advancements of various methods in developing the innovative 3D scaffolds for engineering biomimetic tissue constructs. These techniques include salt leaching (Kim et al., 2017), solvent casting (Choudhury et al., 2015), gas foaming (Nam et al., 2015), freeze-drying (Autissier et al., 2010), and 3D printing, among others (Kankala et al., 2017a, 2018b; An et al., 2015). However, some of these approaches such as solvent casting and others, usually rely on the utilization of large amounts of organic solvents, which may damage the encapsulated sensitive biomolecules in the scaffolds and damage the cells as well as surrounding tissues and provoke the inflammatory responses and other undesirable adverse effects upon implantation (Delmote et al., 2017). Moreover, other limitations include multi-step synthesis (Lee et al., 2016), and complex procedures, which often result in the loss of efficacy of bioactive molecules under high temperature/mechanical stress, reduced loading efficacy of growth regulators due to washing and leaching steps, expensive, irregular porosity and poor mechanical strength of interconnections (Davies et al., 2008; Mao et al., 2012; Rajabzadeh et al., 2012), among others.

Thus, an eco-friendly strategy with controllable processing conditions is necessary to conveniently fabricate a highly porous 3D scaffolds with open and interconnected pores for osteogenic growth and differentiation. The supercritical fluid (SCF) technology, is one such high-pressure eco-friendly technique that has attracted enormous interest in generating polymeric constructs for various biomedical applications such as tissue engineering, drug delivery, imaging, and among other, due to its unique properties such as non-reactive, non-toxic, inflammable, inexpensive, and non-polluting (Kankala et al., 2018c; Moshiri and Oryan, 2012). This technology, by contrast to the aforementioned strategies, takes the advantage of benign solvents such as water and carbon dioxide to replace the organic solvents and thus serving as an effective substitute in fabricating the polymers. In addition, supercritical carbon dioxide (SC-CO_2) is recognized as safe in pharmaceutical processing due to its mild operating conditions, and low toxicity as well as density. Among all the SCFs utilized for polymer processing, SC-CO_2 holds great promise in the fabrication of 3D scaffolds for TE due to ease of its penetration into polymers, high mass transfer, peculiar thermodynamic behavior, interactions with the carbonyl functional groups of polymers (Duarte et al., 2009; Kankala et al., 2017b).

The SC-CO_2-assisted methods for generating 3D porous scaffolds include phase separation (Deng et al., 2013; Yang et al., 2015) and foaming process (Chen et al., 2016; de Matos et al., 2015). Out of these methods, SC-CO_2-assisted foaming of polymers allows the convenient fabrication of scaffolds by not relying on the utilization of organic solvents, which could easily retain the efficacy of biomolecules such as growth factors (Diaz-Gomez et al., 2016a, 2016b; Hile et al., 2000). In addition, it enables the tuning of morphological features of the scaffold by adjusting the processing conditions (i.e., temperature, pressure, processing time, and depressurization rate). However, this strategy yields scaffolds with small-sized and closed porous architectures (Krause et al., 2001), which significantly affect the supply of nutrients, and devoid of adequate space for the adhesion and the migration of cells in the bulk of the scaffold. In addition, it typically results in the formation of a dense superficial layer over the scaffold, which limits the cell adhesion and eventual growth (Singh et al., 2004). In addition, the applicability of this method is limited due to pretreatment of raw materials (de Matos et al., 2013), and longer foaming time, among others (Salerno et al., 2017). Various modifications have been proposed to overcome these limitations by combining with other methods (such as salt leaching) (Jing et al., 2014) to obtain scaffolds with large-sized interconnected pores. However, these methods are quite sophisticated due to multi-step preparation procedures and may suffer from problems that are associated with the efficacy of loaded biomolecules (Salerno et al., 2014a, 2014b).

Inspired by these facts, and to overcome the limitations associated with the traditional supercritical-assisted fabrication methods, we demonstrate the fabrication of polycaprolactone (PCL)-based 3D scaffolds with open and interconnected pores for osteoblast growth and differentiation using an eco-friendly supercritical processing that involves hybrid approaches of phase inversion and foaming (Figure 1). The convenient hybrid processing and the strict optimization of the handling parameters to mild operation levels have facilitated the fabrication of bone morphogenic protein-2 (BMP-2) in the scaffolds. Further, we systematically characterized the prepared scaffolds with various characterization techniques. Subsequently, we demonstrated the effect of scaffolds and loaded growth factor on the adhesion, proliferation and osteogenic differentiation of bone

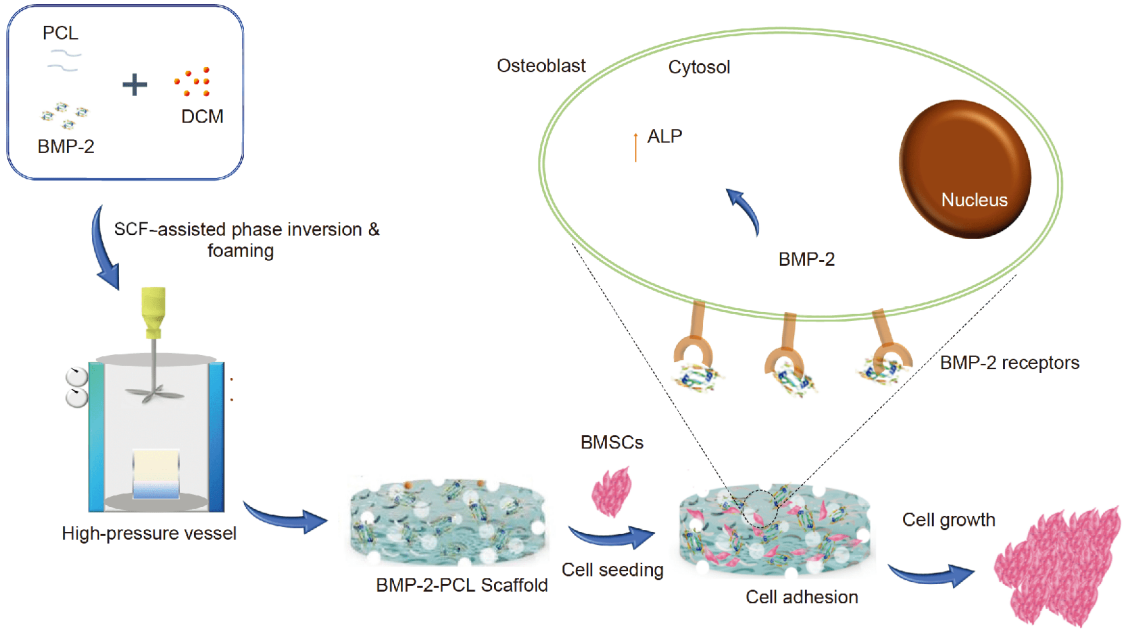

Figure 1 Schematic illustration representing the outline of the preparation of BMP-2-encapsulated PCL scaffolds by supercritical foaming process for bone tissue engineering. Abbreviations: ALP, alkaline phosphatase; BMP-2, bone morphogenic protein-2; BMSCs, bone marrow stromal cells; DCM, dichloromethane; PCL, polycaprolactone.

marrow stromal cells (BMSCs) *in vitro*. Eventually, the osteogenic differentiation was confirmed by analyzing the osteoblast-specific biomarker alkaline phosphatase (ALP).

RESULTS AND DISCUSSION

Porosity and compressive mechanical strength of scaffolds

Initially, the theoretical evaluation of various processing factors (temperature, pressure, and volume of dichloromethane (DCE)) was executed using the Minitab-based experimental design (Tables 1 and 2) and the resultant data of porosity and the mean compressive mechanical strength of the designed scaffolds were compiled in Figure 2. As shown in Figure 2A, the factor A (temperature), as well as factor C (volume of DCM), had shown a significant effect, but factor B (pressure) had shown no noticeable influence on the mean scaffold's porosity. In addition, the porosity plots represented that the porosity of the scaffolds increased with increasing the temperature and volume of DCM (Figure 2B). Similarly, the factor A and C had also shown significant influence on the mean compressive mechanical strength (Figure 2C). Moreover, there were strong interactions between the factors, including AB and BC, which were confirmed in Figure 2D. When factor B was held at a high level, decreasing factor A or increasing factor C, has resulted in the amplification of the compressive mechanical strength. On the other hand, when factor B was held at a low level, decreasing factor A and factor C, resulted in the enhancement of the compressive mechanical strength of the scaffolds. Similar phenomena were observed when holding factor C constant.

Effects of various processing parameters on the scaffold morphology

An ideal scaffold should possess not only fine porosity, that offers immense physical support but also open and interconnected porous architecture for facilitating cell growth. Based on the above results that established the influence of various processing parameters on porosity and compressive mechanical strength of the scaffolds, we carried out the single factor investigation to understand their effects on the morphology of the scaffolds. Figure 3 illustrates the scanning electron microscope (SEM) images of the scaffolds prepared by the supercritical foaming process at various combinations of operating conditions (Table 3). It is evident that the average pore size of the PCL scaffolds was altered with changes in the operating conditions. In this context, the increase in the temperature had resulted in the enhancement of pore size in the beginning and then declined. Moreover, the conditions with respect to the addition of DCM and increase of pressure had also resulted in the significant increase in the pore sizes of the scaffolds. It is evident that the scaffold's morphology and porosity could be regulated by adjusting the addition of DCM and temperature, due to the variation of the mass transfer coefficient of CO_2 and the amount of dissolved CO_2 in the polymer (Fanovich et al., 2013; Lian et al., 2006; Tomasko et al., 2003).

Table 1 Details showing the experimental factors and levels

Level	Code	A Temperature (°C)	B Pressure (bar)	C Volume of DCM (mL)
High level	+1	45	250	0.25
Center point	0	40	200	0.20
Low level	−1	35	150	0.15

Table 2 Experimental results from the factorial design

Run order	A Temperature (°C)	B Pressure (bar)	C Volume of DCM (mL)	Porosity (%)	Compressive mechanical strength (MPa)
1	−1	−1	−1	62.41	2.41
2	1	−1	1	79.52	1.04
3	−1	1	1	69.27	1.68
4	1	1	−1	73.03	1.42
5	1	1	1	81.74	0.61
6	1	−1	−1	71.19	2.15
7	−1	1	−1	64.09	2.34
8	−1	−1	1	75.47	0.78
9	0	0	0	75.75	1.51

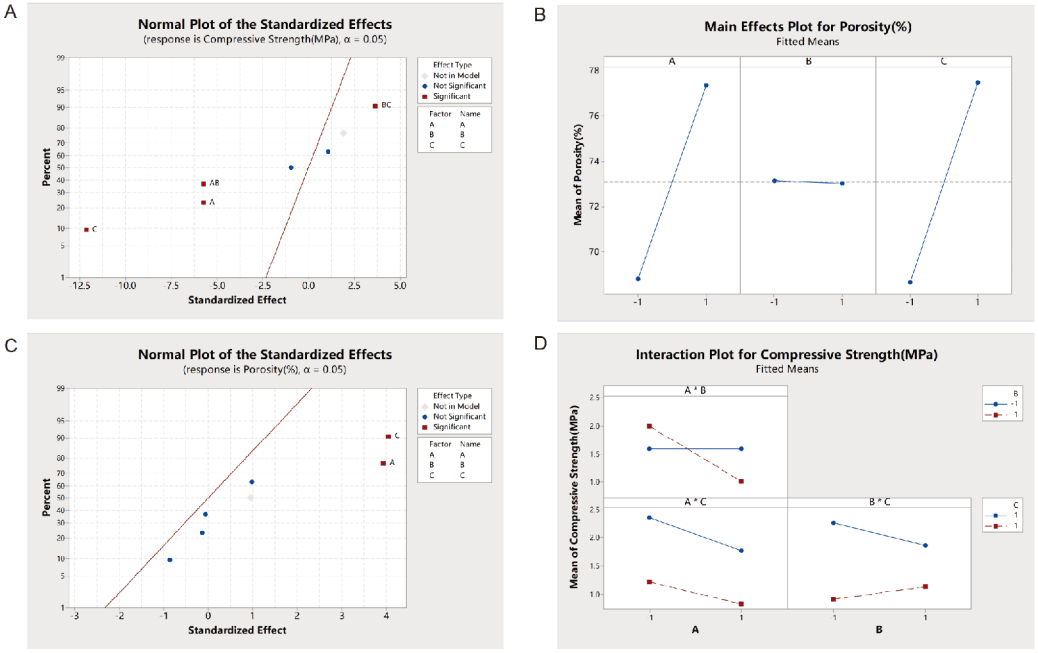

Figure 2 Theoretical assessment through Minitab experiments. A, Standardized effect of the factors on mean scaffold porosity. B, Main effects plot for mean scaffold porosity. C, Standardized effect of the factors on mean compressive mechanical strength. D, Interaction plot for mean compressive mechanical strength.

In this work, we utilized DCM as a co-solvent in the foaming process as it offers numerous advantages such as high compatibility/affinity with the SC-CO_2, enhances the solubility of polymers and easy removal from the end product (Deng et al., 2013; Yang et al., 2015). DCM has been widely used in the preparation of growth factor-loaded microspheres (Qu et al., 2014). There was no significant change or loss in the efficacy of the growth factor. With the addition of DCM, the homogeneous polymer solution underwent a short phase separation process before the foaming process (Figure 4). As shown in Table 2 and Figure 2, the temperature and volume of DCM had a significant effect on the mean scaffold porosity: the porosity generally increased with increasing the temperature and volume of DCM. The obtained

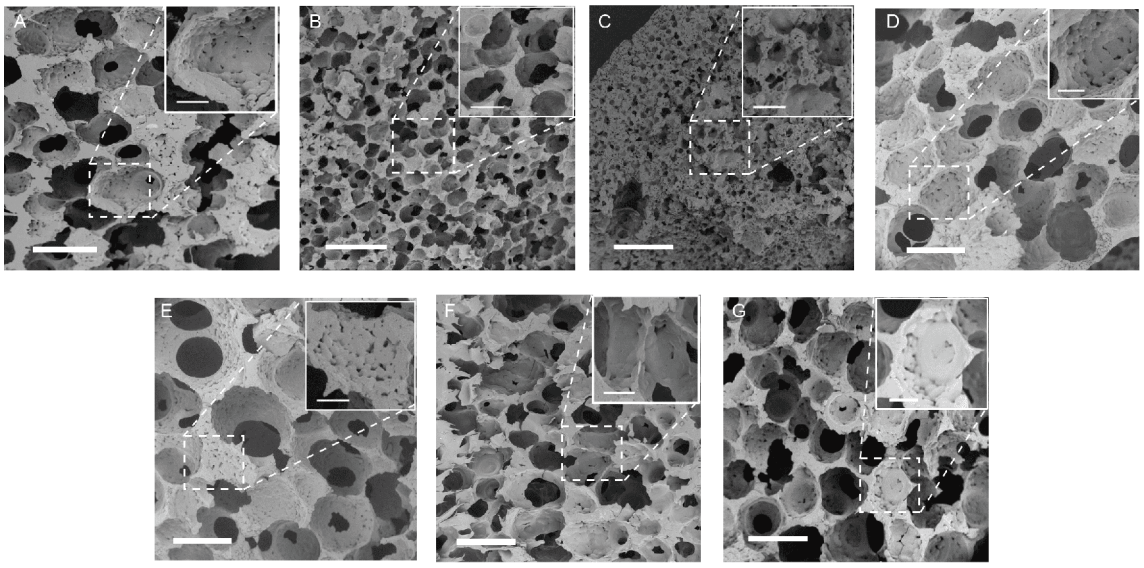

Figure 3 SEM images of the PCL-based 3D scaffolds prepared at various operating conditions, i.e., temperature (°C), volume of DCM (mL) and pressure (bar). A, 40, 0.15, 150; B, 45, 0.15, 150; C, 35, 0.15.150; D, 45, 0.20, 150; E, 45, 0.25, 150; F, 45, 0.15, 200; G, 45, 0.15, 250. Scale bar, 300 μm. Respective inset images showing the magnified view of the scaffolds. Scale bar, 80 μm.

results were in agreement with the previous reports (Chen et al., 2016; Salerno et al., 2014b). Indeed, by elevating the temperature, the system merely results in the reduction of the density of CO_2 after the critical point, which subsequently, diminishes its strength. In addition, the other possible reason is the temperature changes, which might result in the reduction of the viscosity of the solution, yielding the larger pores. Meanwhile, the process of phase separation became slower, and the liquid-liquid phase separation was dominant in the formation of large-sized pores. Together, the porosity of the scaffolds was increased with the increase of temperature and volume of DCM (Tables 2 and 3). Whereas, when the temperature raised up to 45°C, pore sizes in the scaffolds were reduced (Figure 3B). Because of the utilization of DCM as a solvent, the reduced viscosity of PCL in DCM influences the melt strength of PCL, which was not robust enough to support the formation of pore walls. Therefore, the pores might be collapsed before the polymer matrix crystallization (Chen et al., 2016).

In previous studies, (Chen et al., 2016; Fanovich et al., 2013) the results indicated that the pore size was decreased with the increase of pressure both in phase separation and foaming process. In this work, the pressure had shown a little influence on the porosity of the scaffolds (Chen et al., 2016) (Figure 2B). However, the pressure effect on the overall scaffold morphology was slightly different from the above conclusions. Figure 3B, F, and G illustrate that the porous architectures would have collapsed at elevated temperature and pressures due to reduction in viscosity of the solution and the subsequent melt strength were not enough to support the formation of pores (Chen et al., 2016). The resultant enhancement of porosity at the extreme critical conditions might be due to the mobility of PCL matrix that facilitated by high pressures as well as high solubility of CO_2 in PCL, which allowed easy compression and facilitated the pore growth. Moreover, the high pressures in the vessel might lead to decrease in viscosity of the polymer, which was also responsible for the growth of pore, via the pore wall burst and coalescence of nearby pores leading to the formation of interconnected pores (Mathieu et al., 2005). In conclusion, the above effects led to the formation of large and interconnected pores at high pressure. To this end, the results of the full factorial experiment (Table 2) revealed that the porosity was negatively correlated with the compressive strength, which was consistent with the literature (Kim et al., 2017; Mathieu et al., 2005; White et al., 2012). Previous studies indicated that the direction of pores was in the direction of foaming (Mathieu et al., 2006). In this work, the polymer matrix was confined in the mold, and the foams had a specific directivity, which also increased the compressive strength of the scaffolds to a considerable extent.

Physical characterizations

To preserve the growth factor efficacy for osteoblast differentiation, we had chosen the optimized conditions (40°C, 150 bar, 0.15 mL) that resulted in the scaffolds with porosity of 69.02%, compressive strength of 1.82 MPa based on the single factor experiment strategy and further experiments such as systematic physical characterization, growth factor loading and osteogenic differentiation efficacy of scaffolds were designed. Figures 5 and 6 depict the optical image as well as the morphological attributes, revealing the different surfaces of the PCL scaffolds, respectively. Under these

Table 3 Experimental results from the single factor investigation

Run	A Temperature (°C)	B Pressure (bar)	C Volume of DCM (mL)	Pore size (μm) mean ± SD
A	40	150	0.15	200.87±32.61
B	45	150	0.15	109.98±14.09
C	35	150	0.15	33.34±5.46
D	45	150	0.20	236.81±39.26
E	45	150	0.25	309.94±61.53
F	45	200	0.15	190.30±29.95
G	45	250	0.15	203.97±31.84

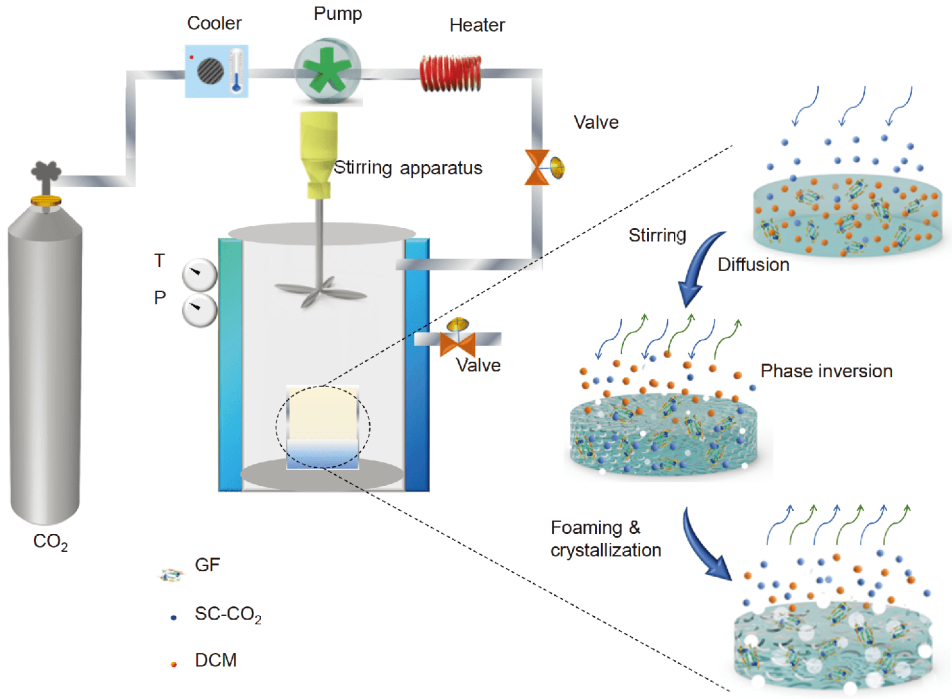

Figure 4 Schematic illustration showing the instrument set-up of the supercritical foaming process.

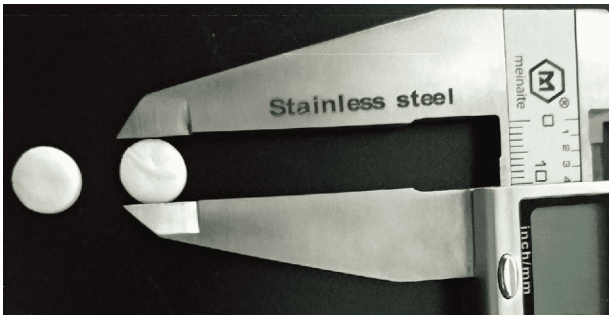

Figure 5 Optical image illustrating the PCL scaffold prepared by supercritical foaming process.

conditions, the addition of DCM was least and the temperature was relatively mild, which has no effect on growth factors (Yano et al., 2009; Qu et al., 2014). In addition, in previous studies (Kim et al., 2017), the results indicated that a scaffold with pores of 180–250 μm might serve as a suitable carrier for cells. As shown in Figure 6, it is evident that the porous structures of the scaffolds were open and interconnected with pore sizes of 200 μm. Accompanied by the phase separation process, the role of DCM was equivalent to that of a porogen in generating the porous architectures. The resultant pores in the scaffolds were formed predominantly due to the escape of DCM during the vigorous stirring of the polymeric mixture. In the subsequent foaming process, DCM played a crucial role as a plasticizer, (Salerno et al., 2014a, 2014b) which was conducive to improving the foaming efficiency. The micropores formed during the phase separation process were used as the nucleation sites for bubble formation, which were beneficial to the nucleation and growth of the pores (Figure 6).

Furthermore, the porous scaffolds were systematically characterized using techniques such as attenuated total re-

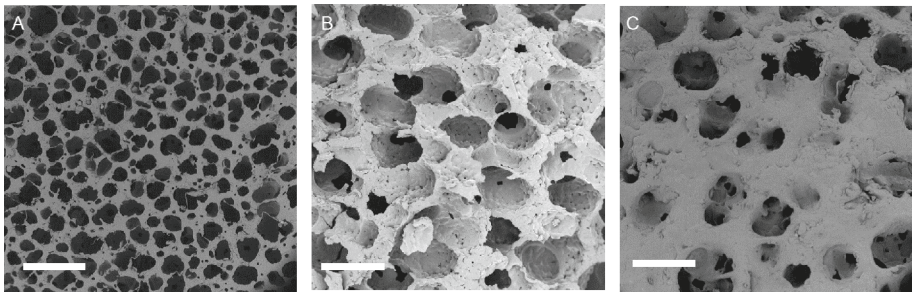

Figure 6 SEM images showing the multidirectional view of the scaffold prepared at the optimized conditions (40°C, 150 bar, 0.15 mL). A, The bottom surface. B, Longitudinal section. C, The top surface. Scale bar, 300 μm.

flectance-Fourier transform infrared spectroscopy (ATR-FTIR), X-ray diffraction (XRD), differential scanning calorimeter (DSC), and the results were compared to that of the raw PCL. To characterize the variations in the functional groups of PCL scaffolds, we employed ATR-FTIR spectroscopic studies to analyze the variations in the chemical structure. Figure 7A depicted that the spectral absorption peaks of raw PCL and PCL scaffolds were almost similar, demonstrating that the SC-CO_2 process had no significant influence on the chemical structure. The XRD patterns of PCL scaffolds are shown in Figure 7B, where the characteristic structural features of them are demonstrated. The characteristic diffractions peaks at 21 and 23 correspond to the basal reflections of d(200) and d(013) planes, which were similar to that of the raw PCL, representing the semi-crystalline domains of PCL. Further, the change in the melting point of PCL scaffolds was also observed. As expected, the melting point of PCL in the scaffolds had shown at around 58.5°C, which slightly lesser than that of raw PCL (60.8°C) (Figure 7C). The shift in the melting temperatures of PCL scaffolds after forming was consistent with the literature, (Salerno et al., 2014a, 2014b) indicating that the supercritical CO_2 assisted process might not significantly influence the crystallinity of PCL.

In this study, the loading efficiency of BMP-2 was measured by using a BMP-2 specific ELISA kit, which was around 26% after supercritical processing. Furthermore, the release of the growth factor was measured. It is evident from the Figure 7D that the porous scaffolds resulted in the sustained release of BMP-2 for about 7 d. Moreover, the release of the loaded BMP-2 from the scaffolds was approximately 41% in 7 d.

In vitro evaluation of the BMP-2 effect on cells grown on the 3D scaffolds

Cell cytotoxicity test

PCL is a biocompatible and biodegradable semi-crystalline polymer approved by FDA in the preparation of medical devices (Woodruff and Hutmacher, 2010). It has been widely used in bone tissue engineering scaffolds. To verify the biocompatibility of PCL scaffolds, we performed the *in vitro* cytotoxicity test using the methyl thiazolyl tetrazolium (MTT) assay, and the results were illustrated in Figure 8B. In addition, these results could also further demonstrate that lower residual amounts of DCM in the scaffolds improve the safety of PCL. It is evident that the DCM residue in the scaffold was only 0.066‰, which was much lower than the limit of the USP 467 Pharmacopeia (0.6‰). Indeed, the MTT experimental results (Figure 8B) demonstrated that the relative viable cell counts measured till 3 days were higher than 90% in different time points, revealing that these scaffolds were highly biocompatible and suitable for biomedical applications.

Cell morphology and cell growth on scaffolds

In this study, we optimized the processing conditions of supercritical foaming process and fabricated the porous scaffolds with excellent porosity, compression strength, and pore structure by surpassing all the problems of traditional foaming process. However, in a few instances, the scaffold still faces certain limitations such as hydrophobicity, lack of cell adhesion, limited cell adhesion, proliferation, and differentiation (Declercq et al., 2013; Lee et al., 2016). Therefore, we introduced BMP-2 into the framework of PCL scaffolds, which play a crucial role in promoting the osteogenic differentiation (Declercq et al., 2013; Lee et al., 2016; Tsuji et al., 2006).

Figure 8A depicts the optical micrographs of the cells that were captured at the respective time intervals to observe the morphologies of BMSCs on the scaffolds after 1, 3 and 7 d of culture. The viability of BMSCs cells on the PCL scaffolds was compared relative to that of the growth of cells on PCL scaffold on Day 1 of incubation (control/quantitative indicator). The cell proliferation rate of all of the groups was increased after incubation for 7 d. As shown in the Figure 8A and E, since the pores are large and interpenetrating, the mass transfer in the scaffold is not hindered, and the cells could be well distributed in the scaffold. Furthermore, the relative viability of cells on the scaffolds was quantified by a cell proliferation test using the cell count kit-8 (CCK-8) assay, and the results were shown in Figure 8C. The cell pro-

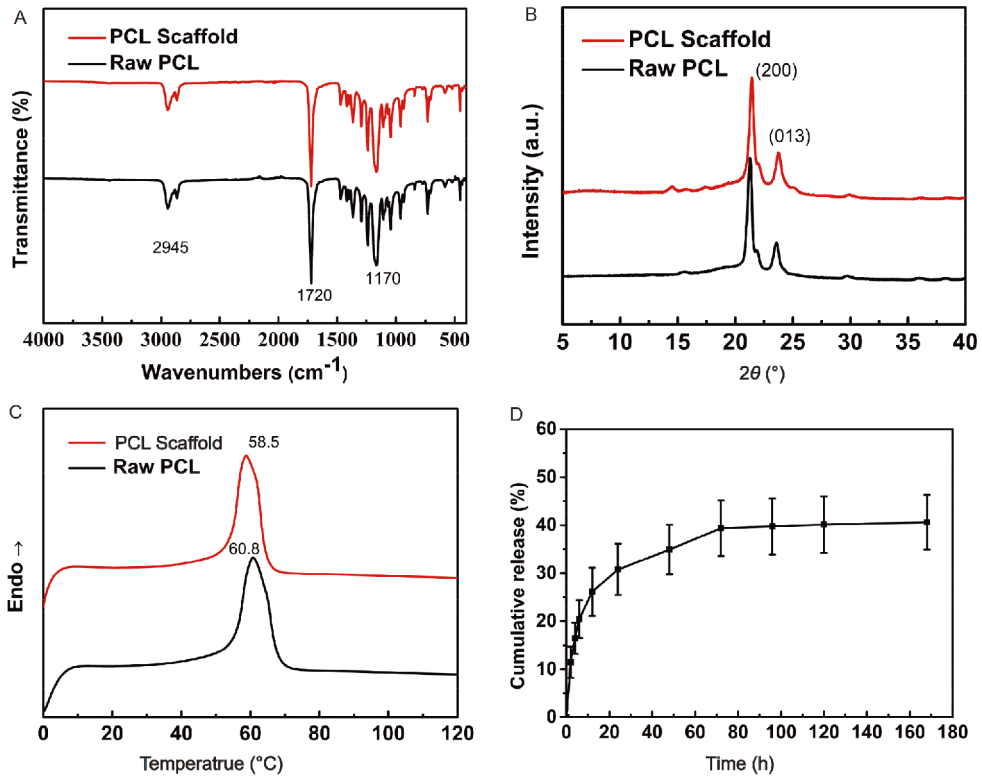

Figure 7 Physicochemical properties of raw PCL and the porous scaffold prepared by the supercritical foaming process. A, FTIR spectra. B, XRD spectra. C, DSC spectra. D, *In vitro* release profile of BMP-2 from the porous scaffolds.

liferation rate of all of the groups increased after incubation for 7 d. Previous studies demonstrated that BMP-2 could induce and enhance adhesion and proliferation of BMSCs on the scaffolds leading to their osteogenic differentiation (Cai et al., 2018; Luo et al., 2017; Shen et al., 2016). Initially (Day 1), the number of cells both on PCL scaffolds and BMP-2-PCL scaffolds displayed a significantly different proliferation rate as compared to that of PCL scaffolds. However, the BMP-2-PCL scaffolds displayed a significantly higher proliferation rate compared to that of PCL scaffolds after 7 d of incubation. The cells treated with the BMP-2 suspended in DMEM has augmented the proliferation rate of cells compared to that of those in the control treatment, but there was no statistically significant difference between the groups at 3 and 7 d.

In vitro osteogenic differentiation of BMSCs

To investigate the osteogenic differentiation of different scaffolds (PCL scaffolds, BMP-2-encapsulated PCL scaffolds (BMP-2-PCL scaffolds) and PCL scaffold in combination with 100 ng mL^{-1} of BMP-2 suspended in DMEM (PCL+BMP-2 in DMEM)) on BMSCs, we quantitatively monitored the ALP amount, as it is an early marker of bone growth. As shown in Figure 8D, the levels of ALP in the treatment of BMP-2-PCL scaffolds treatments were comparatively higher than that of the BMSCs treated with PCL scaffolds. Although BMP-2 in DMEM induced slightly better ALP activity than PCL scaffolds at 7 d, no significant difference was observed between them. These results (Figure 8A and C) suggested that BMP-2 in medium only had a direct effect on cell proliferation in the beginning, while the BMP-2 in scaffold had shown a significant effect on the proliferation of BMSCs in the long run, demonstrating that the sustained release of the growth factor from the scaffolds. It was also evident that this eco-friendly SCF process had no effect on the activity of BMP-2 molecules.

CONCLUSION

We successfully fabricated 3D scaffolds with open and interconnected porous architectures with modified supercritical foaming system for bone tissue engineering. SCF-assisted porous scaffolds exhibited excellent biocompatibility, which was confirmed by cytotoxicity assay. We successfully regulated the morphology, porosity and compressive strength of the scaffold by changing the temperature, pressure, and addition of DCM, with no significant changes in the physical and chemical properties of PCL. These porous scaffolds obtained at optimized, mild supercritical conditions resulted in the efficient encapsulation of BMP-2 growth factor with its activity retained and subse-

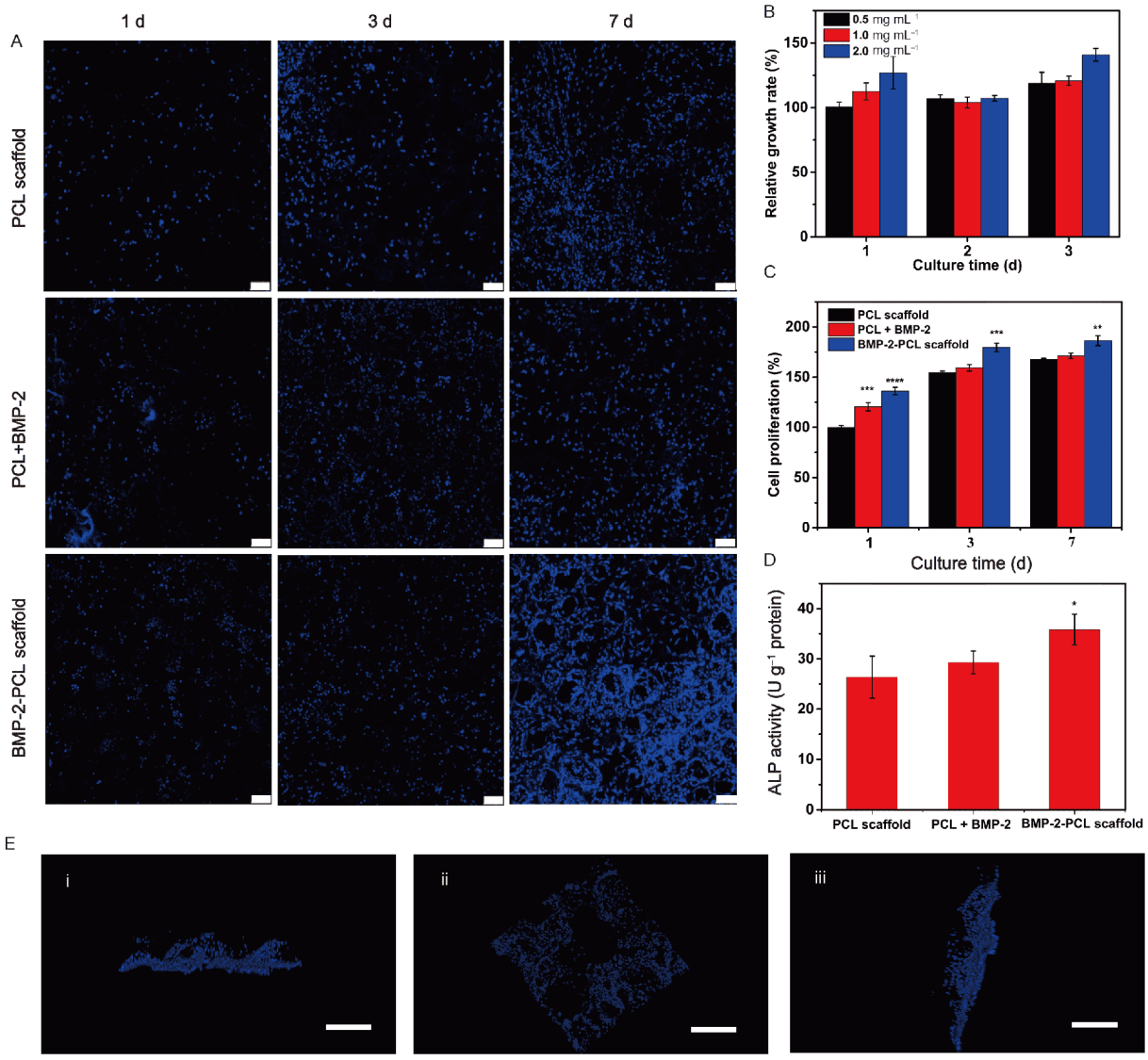

Figure 8 Culture of BMSCs on scaffold. A, BMSCs' morphologies on scaffolds after 1, 3 and 7 d of culture. Scale bar, 100 μm. B, Cell viability of cells after cultured with various concentrations of leaching solution for 1, 2 and 3 d. C, The viability of BMSCs on the scaffolds. D, ALP activity of BMSCs cultured on the scaffolds for 7 d. E, CLSM images representing the 3D view of the scaffold for demonstrating the arrangement of the cells in the porous architectures. (i) Horizontal side view; (ii) top view; (iii) vertical side view, for a real time view. Scale bar, 300 μm. (Movie S1 in Supporting Information).

quently led to its release and eventually cell proliferation and osteogenic differentiation. This technology has a great potential for developing growth factor-encapsulated 3D scaffolds for its delivery in osteogenicity. These innovative scaffolds with excellent physicochemical characteristics will emerge as the promising candidates for bone tissue engineering.

MATERIALS AND METHODS

Materials

BMP-2 powder was purchased from Solar bio-life sciences Co. Ltd. (Beijing China). PCL (average molecular weight of ~100 kD) was purchased from Daigang Biomaterial Co. Ltd. (Jinan, China). Dulbecco's modified Eagle's medium (DMEM), phosphate buffered saline (PBS), fetal bovine serum (FBS), trypsin-ethylenediamine tetraacetic acid (EDTA), penicillin, and streptomycin were purchased from Biological Industries Co. Ltd. (Israel). All other reagents and solvents were of analytical grade and used without further purification.

Fabrication of 3D scaffolds

Scaffolds were prepared in the specially designed polytetrafluoroethylene (PTFE) molds (with a diameter of 1.0 cm and a height of 2.0 cm). 100 mg of PCL was added to the

mold with a certain amount of DCM (0.15 mL) and stirred until it was uniformly dispersed in the solvent and the mold was then placed into the high-pressure vessel. Figure 4 depicts the schematic illustration of the apparatus set up of the supercritical foaming process, which consists of three major components: a CO_2 supply system, a high-pressure vessel with a volume of 104 mL and a mechanical stirrer. SC-CO_2 was pumped into the high-pressure vessel after being adjusted to the desired pressure (150 bar) and temperature (40°C). During this process, the pressure and temperature were kept constant and the solution under stirring (10 r min^{-1}) by a mechanical stirrer. After 3 h of treatment, the stirring device was closed, and the system was rapidly depressurized to atmospheric pressure within 5 min.

Furthermore, the BMP-2 loaded scaffolds (100 ng scaffold^{-1}) were prepared by adding the BMP-2 solution (100 μg mL^{-1} in PBS) along with PCL in the mold, and the preparation was repeated as mentioned above. Eventually, the obtained scaffolds were stored at 4°C. The samples were shortly denoted as BMP-2-PCL scaffolds.

Experimental section

To analyze the effect of the variables of the whole preparation process on the scaffold, first, the key variables were identified as follows: temperature, pressure, and volume of DCM. Further, we investigated the influence and significance of these variables and their effect on the scaffold porosity as well as compressive mechanical strength. To accomplish these tasks, a 2^3 factorial experiment was designed and conducted, and the details were shown in Table 1. Moreover, the levels of the variables were determined on the basis of the pilot experiments. In addition, three experiments at the central point were carried out to estimate the variance in the process. Analysis of the variance was applied to the experimental data using the MINITAB software version 17. Then, an additional single factor experiment was carried out to understand the effects of various process parameters on the morphology of the scaffold.

Physical characterizations

The compressive mechanical properties of the scaffolds were measured on a UTM 6102 (Suns Co. Ltd. Shenzhen, China) equipped with a 0.1 kN loaded cell at room temperature. The cross-head speed was set at 1.0 mm min^{-1} and the compressive strength at 25% strain was determined. Further, the porosity (ε) of each scaffold was calculated by the equation below (Deng et al., 2013; Diaz-Gomez et al., 2016b).

$$\varepsilon = 1 - \rho_s / \rho_p,$$

where ρ_s is the density of the scaffold (scaffold weight/scaffold volume), (g cm^{-3}) and ρ_p is the density of as received PCL (1.11 g cm^{-3}).

DCM residue was measured using a headspace sampler (G1888, Agilent Technologies, USA) coupled to a gas chromatograph (GC) interfaced with a flame ionization detector (6890N, Agilent Technologies, USA) (Deng et al., 2013).

The overall scaffold structure was visualized by SEM measurements. PCL scaffolds were fractured using the liquid nitrogen, and the samples were sputter coated with gold for 40 s. The mean pore size of the foams was evaluated by Nano Measurer software. About one hundred pores for each sample were analyzed.

ATR-FTIR was investigated on NicoletiS10 (Thermo Fisher Scientific, USA) spectrometer, in the range of 4000 to 400 cm^{-1} at room temperature. Spectra were recorded at 4 cm^{-1} spectral resolution with 64 scans. XRD analysis was carried out using a PANalytical X'Pert PRO instrument. The measurement was performed in the range of 5°–40° with a step size of 0.02° in 2θ using Cu Kα radiation as the source. The melting behavior of the scaffolds was investigated by employing a Netzsch DSC 200F3 differential scanning calorimeter. Samples were heated from 0°C to 120°C at a rate of 10°C min^{-1}.

In vitro release studies

The amount of BMP-2 in the PCL scaffold was measured by the reported procedure (Park et al., 2009). Briefly, after preparation of BMP-2-PCL scaffold, 1 mL of PBS was added into a clean microcentrifuge tube, and scaffolds were immersed completely in the PBS. After vortex for 2 min, the supernatant was collected and used to detect the content of free BMP-2 by using BMP-2 ELISA Kit (KeyGEN, Nanjing, China). This process was carried out 4 times. Finally, the scaffolds were dissolved in 5 mL of DCM and the BMP-2 was extracted using PBS. Finally, the amount of BMP-2 was detected by using BMP-2 ELISA Kit.

Further, the release of BMP-2 from the scaffolds was conducted by exposing the BMP-2-PCL scaffolds for a period of 7 d. Initially, the scaffolds were incubated in 1.0 mL of PBS solution and maintained at 37°C, 100 r min^{-1}. At the predetermined time intervals, the aliquots of supernatant were collected and replaced with fresh PBS. The concentration of BMP-2 was determined using the ELISA Kit.

Cell culture

BMSCs were cultured in DMEM that was supplemented with 10% v/v of FBS, and 1% v/v antibiotic/antimycotic solution. The cells were strictly maintained by incubating them at 37°C in 5% CO_2.

Cell viability study

Cell viability was measured by the MTT assay. Typically,

BMSCs were seeded at a density of 5×10^3 cells per well of a 96-well plate and then incubated with the varying concentrations of leaching solution (200 μL) for 1, 2 and 3 d. Next, the culture medium was removed and rinsed twice with PBS. The MTT reagent (10 in 100 μL of freshly prepared culture medium) was added to each well of the 96-well plate and incubated for 4 h to allow the formation of formazan dye. After incubation, the medium was removed, and DMSO (150 μL) was added to solubilize the formazan. The cell viability was then assessed by measuring the absorbance at 570 nm in a microplate reader (SPECTRA MAX, Thermo, USA).

Cell morphology and cell growth on scaffolds

As shown in Figure 5, the scaffolds are regular cylindrical and we used them directly without altering/cutting them into pieces. In addition, the BMSCs were drop seeded onto the bottom of the scaffolds. PCL scaffolds, BMP-2-PCL scaffolds and PCL+BMP-2 in DMEM were sterilized by flushing with 75 vol% of ethanol for 10 min followed by rinsing twice with PBS. Subsequently, the scaffolds were placed in a 48-well plate, and the BMSCs were drop seeded onto the scaffolds at a density of 2×10^5 cells in 40 μL of media per well. After incubation for 2 h, the cell-seeded scaffolds were rinsed twice with PBS, moved onto the fresh 48-well plates to exclude the effect of non-adherent cells. Further, the fresh culture medium (300 μL) was added per well, and the media were replaced every 2 d in all the wells. After culturing the BMSCs for 1, 3, 7 d, respectively, the morphology of cells on scaffolds was visualized by staining with DAPI (KeyGEN, Nanjing, China), which could specifically stain the cell nuclei. Briefly, the cell-seeded scaffolds were rinsed twice with PBS and fixed with 4% of paraformaldehyde for 30 min. The samples were then rinsed thrice again with PBS before staining with DAPI for 8 min. The stained samples were rinsed with PBS, and the images were captured by CLSM (DAPI: λ_{ex}: 405 nm, λ_{em}: 461 nm)

Cell viability on the scaffold was quantitatively analyzed using the CCK-8 (KeyGEN, Nanjing, China) assay according to the manufacturer's instructions. Briefly, after culturing for 1, 3 and 7 d, the original medium was removed and replaced with a CCK-8 solution at a ratio of 1:10 (CCK-8: medium) and incubated for another 4 h at 37°C with 5% CO_2. Thereafter, 100 μL of a solution of each sample was transferred to a 96-well plate and placed in a microplate reader (SPECTRA MAX, Thermo, USA), and then the absorbance of each well was measured at 450 nm.

Alkaline phosphatase activity

ALP activity was quantified as it is an early marker of osteogenic differentiation. Briefly, after 7 d of culture, cell-seeded scaffolds were rinsed with PBS solution, and Radio-Immunoprecipitation Assay (RIPA) buffer (500 μL) was added to each well. The lysate was then transferred to a tube and centrifuged (10,000×*g* at 4°C) for 5 min. ALP activity was quantitatively analyzed using the p-nitrophenol assay (KeyGEN, Nanjing, China) according to the manufacturer's instructions. The collected supernatant or standard solution (30 μL) was mixed with 500 μL of Buffer A and 500 μL of Buffer B and incubated for 30 min at 37°C in the dark. The reaction was stopped by adding 1.5 mL of Buffer C, and the absorbance at 520 nm was measured using the UV-vis spectrophotometer. ALP activity was measured at 520 nm and normalized against the total protein content. The total protein content was measured with a BCA kit (KeyGEN, Nanjing, China) according to the manufacturer's instructions. Briefly, 20 μL of the collected supernatant (the same from ALP activity) was mixed with 200 μL of BCA working reagent and incubated for 15 min at 37°C. Following the incubation, the protein content was measured at 562 nm.

Statistical analysis

All data were presented as the mean ±SD (n=3). The statistical analysis of all the experimental data was performed using GraphPad Prism 7.00. ANOVA single factor analysis was conducted, with the level of statistical significance set at * represents P<0.01, ** represents P<0.005, *** represents P<0.001, **** represents P<0.0001.

Compliance and ethics *The author(s) declare that they have no conflict of interest.*

Acknowledgements *This work was supported by the National Natural Science Foundation of China (U1605225, 31570974, and 31470927), the Public Science and Technology Research Funds Projects of Ocean (201505029), the Promotion Program for Young and Middle-aged Teacher in Science and Technology Research of Huaqiao University (ZQN-PY107) and the Program for Innovative Research Team in Science and Technology in Fujian Province University.*

An, J., Teoh, J.E.M., Suntornnond, R., and Chua, C.K. (2015). Design and 3D printing of scaffolds and tissues. Engineering 1, 261–268.

Autissier, A., Le Visage, C., Pouzet, C., Chaubet, F., and Letourneur, D. (2010). Fabrication of porous polysaccharide-based scaffolds using a combined freeze-drying/cross-linking process. Acta Biomater 6, 3640–3648.

Brydone, A.S., Meek, D., and Maclaine, S. (2010). Bone grafting, orthopaedic biomaterials, and the clinical need for bone engineering. Proc Inst Mech Eng H 224, 1329–1343.

Cabraja, M. and Kroppenstedt, S. (2012). Bone grafting and substitutes in spine surgery. J Neurosurg Sci 56, 87–95.

Cai, Y., Tong, S., Zhang, R., Zhu, T., and Wang, X. (2018). *In vitro* evaluation of a bone morphogenetic protein-2 nanometer hydroxyapatite collagen scaffold for bone regeneration. Mol Med Report 17, 5830.

Cao, Z., Wang, D., Li, Y., Xie, W., Wang, X., Tao, L., Wei, Y., Wang, X., and Zhao, L. (2018). Effect of nanoheat stimulation mediated by magnetic nanocomposite hydrogel on the osteogenic differentiation of mesenchymal stem cells. Sci China Life Sci 61, 448–456.

Chen, B., Kankala, R.K., Chen, A., Yang, D., Cheng, X., Jiang, N., Zhu, K., and Wang, S. (2017). Investigation of silk fibroin nanoparticle-decorated poly(L-lactic acid) composite scaffolds for osteoblast growth and differentiation. Int J Nanomed 12, 1877–1890.

Chen, C., Liu, Q., Xin, X., Guan, Y., and Yao, S. (2016). Pore formation of poly(ε-caprolactone) scaffolds with melting point reduction in supercritical CO_2 foaming. J Supercrit Fluids 117, 279–288.

Choudhury, M., Mohanty, S., and Nayak, S. (2015). Effect of different solvents in solvent casting of porous pla scaffolds—in biomedical and tissue engineering applications. J Biomater Tissue Eng 5, 1–9.

Custódio, C.A., Reis, R.L., and Mano, J.F. (2014). Engineering biomolecular microenvironments for cell instructive biomaterials. Adv Healthc Mater 3, 797–810.

Davies, O.R., Lewis, A.L., Whitaker, M.J., Tai, H., Shakesheff, K.M., and Howdle, S.M. (2008). Applications of supercritical CO_2 in the fabrication of polymer systems for drug delivery and tissue engineering. Adv Drug Deliver Rev 60, 373–387.

Delmote, J., Teruel-Biosca, L., Gómez Ribelles, J.L., and Gallego Ferrer, G. (2017). Emulsion based microencapsulation of proteins in poly(L-lactic acid) films and membranes for the controlled release of drugs. Polym Degrad Stabil 146, 24–33.

de Matos, M.B.C., Piedade, A.P., Alvarez-Lorenzo, C., Concheiro, A., Braga, M.E.M., and de Sousa, H.C. (2013). Dexamethasone-loaded poly(-caprolactone)/silica nanoparticles composites prepared by supercritical CO_2 foaming/mixing and deposition. Int J Pharm 456, 269–281.

de Matos, M.B.C., Puga, A.M., Alvarez-Lorenzo, C., Concheiro, A., Braga, M.E.M., and de Sousa, H.C. (2015). Osteogenic poly(ε-caprolactone)/poloxamine homogeneous blends prepared by supercritical foaming. Int J Pharm 479, 11–22.

Declercq, H.A., Desmet, T., Berneel, E.E.M., Dubruel, P., and Cornelissen, M.J. (2013). Synergistic effect of surface modification and scaffold design of bioplotted 3-D poly-ε-caprolactone scaffolds in osteogenic tissue engineering. Acta Biomater 9, 7699–7708.

Deng, A., Chen, A., Wang, S., Li, Y., Liu, Y., Cheng, X., Zhao, Z., and Lin, D. (2013). Porous nanostructured poly-L-lactide scaffolds prepared by phase inversion using supercritical CO_2 as a nonsolvent in the presence of ammonium bicarbonate particles. J Supercrit Fluids 77, 110–116.

Diaz-Gomez, L., Concheiro, A., Alvarez-Lorenzo, C., and García-González, C.A. (2016a). Growth factors delivery from hybrid PCL-starch scaffolds processed using supercritical fluid technology. Carbohyd Polym 142, 282–292.

Diaz-Gomez, L., Yang, F., Jansen, J.A., Concheiro, A., Alvarez-Lorenzo, C., and García-González, C.A. (2016b). Low viscosity-PLGA scaffolds by compressed CO_2 foaming for growth factor delivery. RSC Adv 6, 70510–70519.

Duarte, A.R.C., Mano, J.F., and Reis, R.L. (2009). Perspectives on: supercritical fluid technology for 3D tissue engineering scaffold applications. J Bioact Compat Polym 24, 385–400.

Fanovich, M.A., Ivanovic, J., Misic, D., Alvarez, M.V., Jaeger, P., Zizovic, I., and Eggers, R. (2013). Development of polycaprolactone scaffold with antibacterial activity by an integrated supercritical extraction and impregnation process. J Supercrit Fluids 78, 42–53.

Hegde, C., Shetty, V., Wasnik, S., Ahammed, I., and Shetty, V. (2013). Use of bone graft substitute in the treatment for distal radius fractures in elderly. Eur J Orthop Surg Traumatol 23, 651–656.

Hile, D.D., Amirpour, M.L., Akgerman, A., and Pishko, M.V. (2000). Active growth factor delivery from poly(D,L-lactide-co-glycolide) foams prepared in supercritical CO_2. J Control Releas 66, 177–185.

Jing, X., Mi, H., Cordie, T., Salick, M., Peng, X., and Turng, L.S. (2014). Fabrication of porous poly(ε-caprolactone) scaffolds containing chitosan nanofibers by combining extrusion foaming, leaching, and freeze-drying methods. Ind Eng Chem Res 53, 17909–17918.

Kankala, R.K., Zhu, K., Li, J., Wang, C., Wang, S., and Chen, A. (2017a). Fabrication of arbitrary 3D components in cardiac surgery: from macro-, micro- to nanoscale. Biofabrication 9, 032002.

Kankala, R.K., Zhang, Y., Wang, S., Lee, C.H., and Chen, A. (2017b). Supercritical fluid technology: an emphasis on drug delivery and related biomedical applications. Adv Healthc Mater 6, 1700433.

Kankala, R.K., Zhu, K., Sun, X., Liu, C., Wang, S., and Chen, A. (2018a). Cardiac tissue engineering on the nanoscale. ACS Biomater Sci Eng 4, 800–818.

Kankala, R.K., Xu, X., Liu, C., Chen, A., and Wang, S. (2018b). 3D-printing of microfibrous porous scaffolds based on hybrid approaches for bone tissue engineering. Polymers 10, 807.

Kankala, R.K., Chen, B., Liu, C., Tang, H., Wang, S., and Chen, A. (2018c). Solution-enhanced dispersion by supercritical fluids: an ecofriendly nanonization approach for processing biomaterials and pharmaceutical compounds. Int J Nanomed 13, 4227–4245.

Kim, H.Y., Kim, H.N., Lee, S.J., Song, J.E., Kwon, S.Y., Chung, J.W., Lee, D., and Khang, G. (2017). Effect of pore sizes of PLGA scaffolds on mechanical properties and cell behaviour for nucleus pulposus regeneration *in vivo*. J Tissue Eng Regen Med 11, 44–57.

Krause, B., Mettinkhof, R., van der Vegt, N.F.A., and Wessling, M. (2001). Microcellular foaming of amorphous high-T_g polymers using carbon dioxide. Macromolecules 34, 874–884.

Lee, S.J., Lee, D., Yoon, T.R., Kim, H.K., Jo, H.H., Park, J.S., Lee, J.H., Kim, W.D., Kwon, I.K., and Park, S.A. (2016). Surface modification of 3D-printed porous scaffolds via mussel-inspired polydopamine and effective immobilization of rhBMP-2 to promote osteogenic differentiation for bone tissue engineering. Acta Biomater 40, 182–191.

Lenas, P., and Ikonomou, L. (2018). Developmental engineering: design of clinically efficacious bioartificial tissues through developmental and systems biology. Sci China Life Sci 61, 978–981.

Lian, Z., Epstein, S.A., Blenk, C.W., and Shine, A.D. (2006). Carbon dioxide-induced melting point depression of biodegradable semicrystalline polymers. J Supercrit Fluids 39, 107–117.

Luo, G., Huang, Y., and Gu, F. (2017). RhBMP2-loaded calcium phosphate cements combined with allogenic bone marrow mesenchymal stem cells for bone formation. Biomed Pharmacother 92, 536–543.

Mao, J., Duan, S., Song, A., Cai, Q., Deng, X., and Yang, X. (2012). Macroporous and nanofibrous poly(lactide-co-glycolide)(50/50) scaffolds via phase separation combined with particle-leaching. Mater Sci Eng-C 32, 1407–1414.

Mathieu, L.M., Montjovent, M.O., Bourban, P.E., Pioletti, D.P., and Månson, J.A.E. (2005). Bioresorbable composites prepared by supercritical fluid foaming. J Biomed Mater Res 75A, 89–97.

Mathieu, L.M., Mueller, T.L., Bourban, P.E., Pioletti, D.P., Müller, R., and Månson, J.A.E. (2006). Architecture and properties of anisotropic polymer composite scaffolds for bone tissue engineering. Biomaterials 27, 905–916.

Moshiri, A., and Oryan, A. (2012). Role of tissue engineering in tendon reconstructive surgery and regenerative medicine: current concepts, approaches and concerns. Hard Tissue 1, 11.

Nam, Y.S., Yoon, J.J., and Park, T.G. (2015). A novel fabrication method of macroporous biodegradable polymer scaffolds using gas foaming salt as a porogen additive. J Biomed Mater Res 53, 1–7.

Oryan, A., Alidadi, S., Moshiri, A., and Maffulli, N. (2014). Bone regenerative medicine: classic options, novel strategies, and future directions. J Orthop Surg Res 9, 18.

Park, K.H., Kim, H., Moon, S., and Na, K. (2009). Bone morphogenic protein-2 (BMP-2) loaded nanoparticles mixed with human mesenchymal stem cell in fibrin hydrogel for bone tissue engineering. J Biosci Bioeng 108, 530–537.

Qu, X., Cao, Y., Chen, C., Die, X., and Kang, Q. (2014). A poly(lactide-co-glycolide) film loaded with abundant bone morphogenetic protein-2: a substrate-promoting osteoblast attachment, proliferation, and differentiation in bone tissue engineering. J Biomed Mater Res 103, 2786–2796.

Rajabzadeh, S., Liang, C., Ohmukai, Y., Maruyama, T., and Matsuyama, H. (2012). Effect of additives on the morphology and properties of poly (vinylidene fluoride) blend hollow fiber membrane prepared by the thermally induced phase separation method. J Membrane Sci 423–424, 189–194.

Salerno, A., Clerici, U., and Domingo, C. (2014a). Solid-state foaming of biodegradable polyesters by means of supercritical CO_2/ethyl lactate mixtures: towards designing advanced materials by means of sustainable processes. Eur Polymer J 51, 1–11.

Salerno, A., Fanovich, M.A., and Pascual, C.D. (2014b). The effect of ethyl-lactate and ethyl-acetate plasticizers on PCL and PCL-HA composites foamed with supercritical CO_2. J Supercrit Fluids 95, 394–406.

Salerno, A., Diéguez, S., Diaz-Gomez, L., Gómez-Amoza, J.L., Magariños, B., Concheiro, A., Domingo, C., Alvarez-Lorenzo, C., and García-González, C.A. (2017). Synthetic scaffolds with full pore interconnectivity for bone regeneration prepared by supercritical foaming using advanced biofunctional plasticizers. Biofabrication 9, 035002.

Shen, X., Zhang, Y., Gu, Y., Xu, Y., Liu, Y., Li, B., and Chen, L. (2016). Sequential and sustained release of SDF-1 and BMP-2 from silk fibroin-nanohydroxyapatite scaffold for the enhancement of bone regeneration. Biomaterials 106, 205–216.

Singh, L., Kumar, V., and Ratner, B.D. (2004). Generation of porous microcellular 85/15 poly (DL-lactide-co-glycolide) foams for biomedical applications. Biomaterials 25, 2611–2617.

Tomasko, D.L., Li, H., Liu, D., Han, X., Wingert, M.J., Lee, L.J., and Koelling, K.W. (2003). A review of CO_2 applications in the processing of polymers. Ind Eng Chem Res 42, 6431–6456.

Tsuji, K., Bandyopadhyay, A., Harfe, B.D., Cox, K., Kakar, S., Gerstenfeld, L., Einhorn, T., Tabin, C.J., and Rosen, V. (2006). BMP2 activity, although dispensable for bone formation, is required for the initiation of fracture healing. Nat Genet 38, 1424–1429.

White, L.J., Hutter, V., Tai, H., Howdle, S.M., and Shakesheff, K.M. (2012). The effect of processing variables on morphological and mechanical properties of supercritical CO_2 foamed scaffolds for tissue engineering. Acta Biomater 8, 61–71.

Woodruff, M.A., and Hutmacher, D.W. (2010). The return of a forgotten polymer—polycaprolactone in the 21st century. Prog Polymer Sci 35, 1217–1256.

Xie, Y., Song, W., Zhao, W., Gao, Y., Shang, J., Hao, P., Yang, Z., Duan, H., and Li, X. (2018). Application of the sodium hyaluronate-cntf scaffolds in repairing adult rat spinal cord injury and facilitating neural network formation. Sci China Life Sci 61, 559–568.

Yano, K., Hoshino, M., Ohta, Y., Manaka, T., Naka, Y., Imai, Y., Sebald, W., and Takaoka, K. (2009). Osteoinductive capacity and heat stability of recombinant human bone morphogenetic protein-2 produced by *Escherichia coli* and dimerized by biochemical processing. J Bone Miner Metab 27, 355–363.

Yang, D., Chen, A., Wang, S., Li, Y., Tang, X., and Wu, Y. (2015). Preparation of poly(L-lactic acid) nanofiber scaffolds with a rough surface by phase inversion using supercritical carbon dioxide. Biomed Mater 10, 035015.

Zeltinger, J., Sherwood, J.K., Graham, D.A., Müeller, R., and Griffith, L.G. (2001). Effect of pore size and void fraction on cellular adhesion, proliferation, and matrix deposition. Tissue Eng 7, 557–572.

Zhao, G., Cao, Y., Zhu, X., Tang, X., Ding, L., Sun, H., Li, J., Li, X., Dai, C., Ru, T., et al. (2017). Transplantation of collagen scaffold with autologous bone marrow mononuclear cells promotes functional endometrium reconstruction via downregulating ΔNp63 expression in Asherman's syndrome. Sci China Life Sci 60, 404–416.

SUPPORTING INFORMATION

Movie S1 Culture of BMSCs.

The supporting information is available online at http://life.scichina.com and https://link.springer.com. The supporting materials are published as submitted, without typesetting or editing. The responsibility for scientific accuracy and content remains entirely with the authors.